# Perovskite-based heterostructures integrating ferromagnetic-insulating $La_{0.1}Bi_{0.9}MnO_3$

M. Gajek
*Instituto de Ciencia de Materiales de Barcelona-Consejo Superior de Investigaciones Cientificas (ICMAB-CSIC), Campus de la Universitat Autonoma de Barcelona (UAB), Bellaterra 08193, Catalunya, Spain and Unité Mixte de Physique Centre National de la Recherche Scientifique-THALES (CNRS-THALES), Universite Paris-Sud, Domaine de Corbeville, Orsay, 91404 France*

M. Bibes[a)]
*Institut d'Electronique Fondamentale, Université Paris-Sud, Orsay 91405, France*

A. Barthélémy
*Unité Mixte de Physique Centre National de la Recherche-THALES (CNRS-THALES), Université Paris-Sud, Domaine de Corbeville, Orsay 91404, France*

M. Varela
*Departamento de Física Aplicada i Òptica, Universitat de Barcelona, Diagonal 647, 08028 Barcelona, Catalunya, Spain*

J. Fontcuberta
*Instituto de Ciencia de Materials de Barcelona-Consejo de Investigaciones Cientificas (ICMAB-CSIC), Campus de la Universitat Autonoma de Barcelona (UAB), Bellaterra 08193, Catalunya, Spain*

(Received 12 July 2004; accepted 8 March 2005; published online 6 May 2005)

We report on the growth of thin films and heterostructures of the ferromagnetic-insulating perovskite $La_{0.1}Bi_{0.9}MnO_3$. We show that the $La_{0.1}Bi_{0.9}MnO_3$ perovskite grows single phased, epitaxially, and with a single out-of-plane orientation either on $SrTiO_3$ substrates or onto strained $La_{2/3}Sr_{1/3}MnO_3$ and $SrRuO_3$ ferromagnetic-metallic buffer layers. We discuss the magnetic properties of the $La_{0.1}Bi_{0.9}MnO_3$ films and heterostructures in view of their possible potential as magnetoelectric or spin-dependent tunneling devices. © *2005 American Institute of Physics*. [DOI: 10.1063/1.1899227]

## I. INTRODUCTION

An increasing number of studies have been recently published on the growth and physical properties of magnetoelectric (or biferroic) materials.[1] In these systems, ferro(antiferro)electric and ferro(antiferro)magnetic orders coexist, with some coupling between them.[2] This may allow one to control the ferroelectric properties of such compounds through the application of a magnetic field[3,4] and, alternately, to control their magnetic properties through the application of an electric field. Most of these studies, however, have searched for such effects in bulk samples, and little work has been done up to now on thin films.[5]

In this article, we report on the growth of films and heterostructures of the ferromagnetic-insulating perovskite $La_{0.1}Bi_{0.9}MnO_3$ (LBMO). Although very little is known on this material, even in bulk form,[6] it can be anticipated that it shares magnetoelectric properties with its parent $BiMnO_3$ (a ferromagnetic and ferroelectric) for which a clear magnetocapacitance effect, resulting from a coupling between the two ferroic orders, has been evidenced.[7] This latter system has been grown in thin-film form by a few groups[8,9] but nothing has been reported as to its integration into heterostructures. For this study, we have focused on La-substituted $BiMnO_3$, aiming to overcome the difficulty of stabilizing the $BiMnO_3$ phase in thin films and concomitantly avoiding the presence of parasite phases. Indeed, the preparation of single-phase $BiMnO_3$ bulk samples requires high pressure, while La-substituted ($La_xBi_{1-x}MnO_3$) compounds can be prepared in 1 atm, for $x > 0.3$ (Ref. 6). It thus appears that the partial substitution of Bi by La favors the stabilization of the desired phase. In the present work, the level of the La substitution is only 10% but, as will be demonstrated, this is enough to allow the stabilization of the pure LBMO phase through epitaxy, avoiding the presence of spurious Bi-rich phases that show up when trying to grow $BiMnO_3$ films from a stoichiometric target.[10]

We thus report here the growth and structural properties of LBMO single films as well as those of LBMO films grown onto $La_{2/3}Sr_{1/3}MnO_3$ (LSMO) and $SrRuO_3$ (SRO) buffer layers. These materials are both metallic and ferromagnetic and can be used as electrodes in devices in which the LBMO layer would be the key element. We show that our LBMO films are single phased, epitaxial, and ferromagnetic and that, under appropriate conditions, a magnetic decoupling can be achieved between the LBMO and the buffer layer in the heterostructures, thus fulfilling the prerequisite for the use of such heterostructures as magnetoelectric or spin-dependent tunneling devices.

[a)]Author to whom correspondence should be addressed; electronic mail: manuel.bibes@ief.u-psud.fr

 

## II. EXPERIMENTAL

### A. Growth

LBMO epitaxial layers as well as SRO/LBMO and LSMO/LBMO bilayers were deposited on $SrTiO_3$ (001) substrates by pulsed laser deposition (PLD) using a KrF ($\lambda = 248$ nm) laser with a fluence of 2 $J/cm^2$ at a repetition rate of 2 Hz. LBMO layers were grown in an $O_2$ pressure of $1.10^{-1}$ mbar and the substrate temperature was set to 650 °C while SRO and LSMO buffers were respectively deposited at 675 °C and 700 °C with an oxygen pressure of 0.2 mbar. A stoichiometric mixture of sintered $La_2O_3$, $Bi_2O_3$, and $MnO_2$ powders was used to produce the target for LBMO. The oxygen pressure was increased to 1 bar after deposition while cooling the samples in order to preserve the oxygen content.

No data exist on the structure of bulk LBMO, but we can speculate that it is close to that of $BiMnO_3$. This latter compound is a heavily distorted perovskite with a monoclinic symmetry (C2 space group, $a_m = 9.54$ Å, $c_m = 9.86$ Å, $b_m = 5.61$ Å, $\alpha_m = \beta_m = 90°$, $\gamma_m = 110.7°$, where $m$ index is for monoclinic),[11] which can also be represented in a pseudotriclinic system ($a_t = c_t = 3.93$ Å, $b_t = 3.99$ Å, $\alpha_t = \gamma_t = 90.4°$, $\beta_t = 91.4°$, where $t$ index is for triclinic). In the following, for the sake of clarity, we will assume the structural parameters of bulk LBMO to be the same as those of BMO. $SrTiO_3$ (STO) is a cubic material with a unit-cell parameter of 3.905 Å, which should induce a compressive strain state on the LBMO films. The mismatch is $-0.64\%$ with LBMO $a_t$ and $c_t$ cell parameters, and $-2.1\%$ with $b_t$. Although taking the pseudotriclinic representation to describe the growth of the LBMO phase is inaccurate as it conceals the real symmetry of the material (monoclinic), it gives a good estimation of the stresses that come into play between the film and the substrate. From these considerations, a strong preference for $b_t$-oriented growth is expected.

Unless otherwise specified, the thickness of the different layers (checked by x-ray reflectometry) was set to 30 nm for LBMO, 50 nm for SRO, and 50 nm for LSMO.

### B. Physical measurements

Structural determinations were carried out by x-ray diffraction in a Philips MRD four-circle diffractometer system. Thickness has been evaluated by x-ray reflectivity measurements on a Rigaku Rotaflex RU-200B diffractometer. Morphological characterization was done with a Molecular Imaging PicoSPM atomic force microscope (AFM) in a tapping mode. Magnetic measurements were performed with the field applied along STO[100] in a Quantum Design superconducting quantum device interferometer (SQUID).

## III. RESULTS AND DISCUSSION

### A. Structure

As can be judged from the $\theta$-2 $\theta$ scan presented in Fig. 1, x-ray diffraction experiments performed on LBMO single films grown on STO did not evidence the presence of parasite phases and all the peaks could be indexed with the $(00l)_c$ reflections of STO ($c$ for cubic indexation) and $(\bar{l}0l)_m$ of

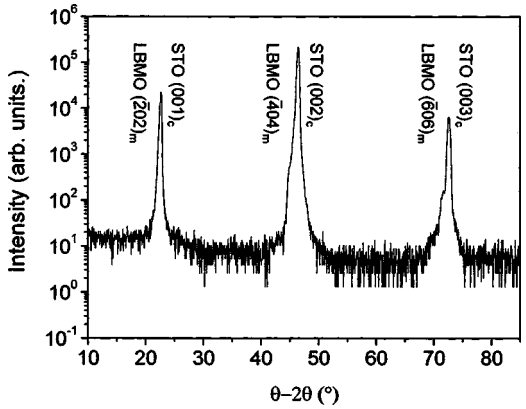


FIG. 1. $\theta$-2 $\theta$ scan for a LBMO film grown on STO.

LBMO ($m$ for monoclinic indexation). The $(\bar{l}0l)_m$ reflections correspond to the $(0l0)_t$ reflections, and thus the film is $b$-oriented in the triclinic indexation, as expected from elastic energy considerations. As opposed to what was found by Moreira dos Santos *et al.*[9] for BMO films grown on STO, no $(111)_m$-, $(101)_m$-, or $(311)_m$-oriented crystallites were detected. Our LBMO films thus appears to be single phased with only one structural out-of-plane orientation. In Fig. 2(a), we show a $\theta$-2 $\theta$ scan close to the $(002)_c$ reflection ($c$ for cubic indexation) of STO for a LBMO single film (bottom curve). The peak at 46.00° is attributed to the $(40\bar{4})_m$ reflection of the LBMO phase. In this figure, we also show the scan for a LSMO single film grown on STO(001) (middle curve). The peak at 47.32° corresponds to the $(002)_c$ reflection of LSMO (pseudocubic notation) from which we deduce an out-of-plane parameter $c_{c-\mathrm{LSMO}}$ of 3.846 Å. This value is lower than the parameter of bulk LSMO (3.88 Å), which is consistent with a tensile strain state imposed by the STO. In the top curve, we show the $\theta$-2 $\theta$ scan of a LSMO/LBMO bilayer. In the full-range spectrum (not shown), all the peaks could be indexed with the $(\bar{l}0l)_m$-type reflections of LBMO

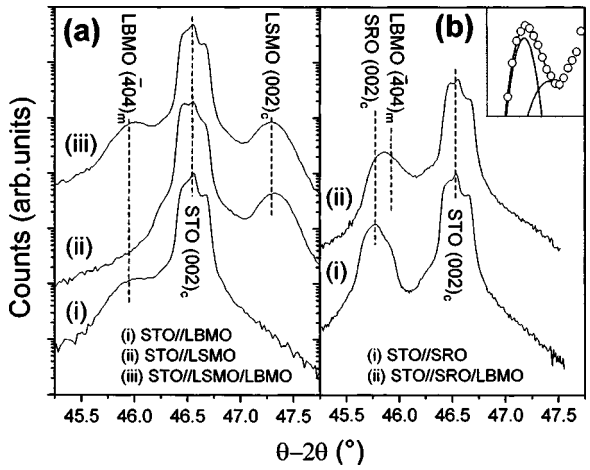


FIG. 2. (a) $\theta$-2 $\theta$ scan close to the $(002)_c$ reflection of STO for a single LBMO layer (i), a single LSMO layer (ii), and a LSMO/LBMO bilayer. (b) $\theta$-2 $\theta$ scan close to the $(002)_c$ reflection of STO for a single SRO layer (i) and a SRO/LBMO bilayer (ii). Inset: zoom of the peak attributed to the $(002)_c$ reflection of SRO and the $(40\bar{4})_m$ reflection of LBMO; the experimental data are shown as open circles, and the fit results as solid lines.

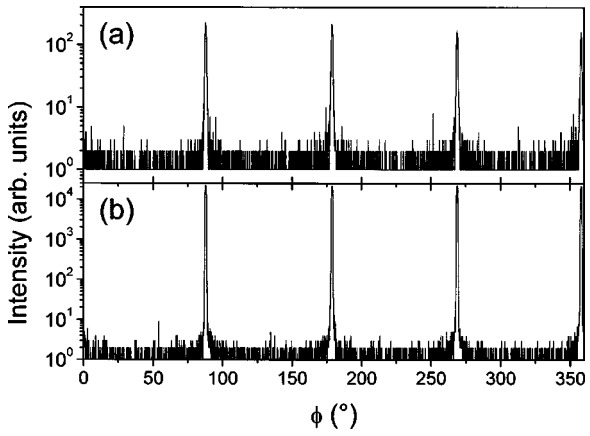


FIG. 3. $\phi$ scan of the (a) $(\bar{7}15)_m$ reflection of LBMO and (b) (031) reflection of STO for a LBMO single film.

and the $(00l)_c$-type reflections of LSMO and STO, with no indication of extraphases. In the curve shown here, the peaks corresponding to the $(40\bar{4})_m$ reflection of LBMO and to the $(002)_c$ reflection of LSMO can be clearly identified at $2\theta = 46.00°$ and $2\theta = 47.32°$ respectively. These values are coincident with those of the corresponding single films and thus it follows that the LSMO and the LBMO layers are in a similar strain state in the single films and in the heterostructure.

In Fig. 2(b), we show results from a similar analysis for a SRO/LBMO bilayer. The lower spectrum corresponds to the $\theta$-$2\theta$ scan of a single SRO film grown on STO. The peak at 45.76 ° can be attributed to the $(002)_c$ reflection (pseudocubic notation) of the SRO single layer. We deduce an out-of-plane parameter $c_{c\text{-SRO}} = 3.962$ Å, consistent with a heavily strained (compressive) state ($c_{c\text{-bulk SRO}} = 3.93$ Å). In this figure, the top curve corresponds to a SRO/LBMO bilayer and shows a peak at 45.86 °, attributed to the $(002)_c$ reflection of SRO. This peak is thus slightly shifted to higher angles with respect to its equivalent in the single film. By fitting the x-ray spectrum with Gaussian lines (see inset), one can show that this is partly due to an effect of convolution with the $(40\bar{4})_m$ peak of LBMO. From this analysis, we deduce that the exact angular position of the SRO peak is 45.84 ° ($c_{c-\text{SRO}} = 3.956$ Å, i.e., very close to the parameter obtained for the single SRO film), and that of the LBMO peak is 46.07 °, reflecting a slightly smaller $(40\bar{4})_m$ lattice spacing than in the single LBMO film. Reciprocal space mappings (not shown) around the $(204)_c$ reflection of STO indeed reveal a virtually fully strained state for the SRO and LBMO layers, within experimental resolution. In both bilayers, the full width at half maximum (FWHM) of the rocking curve of $(40\bar{4})_m$ LBMO's peak was 0.13 °, evidencing a highly textured growth quality.

In Fig. 3, we show $\phi$ scans of the $(\bar{7}15)_m$ reflection of LBMO (which corresponds to the $(130)_t$ reflection) and the $(103)_c$ reflection of STO for a LBMO single film. The periodicity of the peaks and their positions are the same for both material and no doubling of the peaks could be detected within our experimental resolution. Thus there is no evidence for the presence of multiple in-plane orientations for the LBMO film, irrespective of the presumed monoclinic symmetry of the bulk compound. The film is therefore assumed to grow pseudocube-on-cube onto the substrate. Similar results were obtained for LBMO layers integrated into heterostructures.

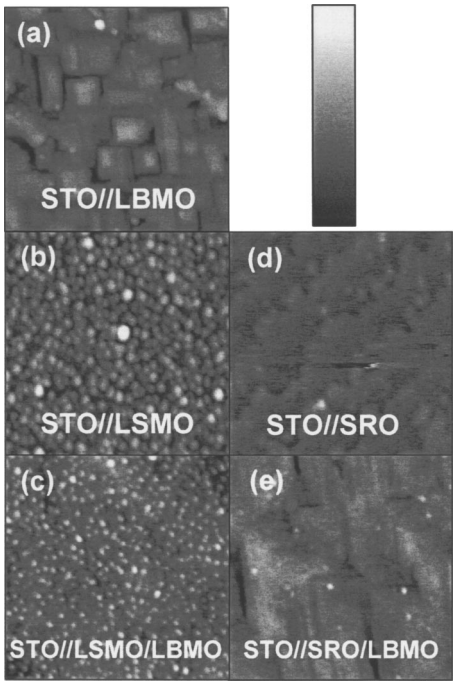


FIG. 4. 1-$\mu$m$^2$ AFM scans of (a) a single LBMO layer, (b) a single LSMO layer, (c) a LSMO/LBMO bilayer, (d) a single SRO layer, and (e) a SRO/LBMO bilayer. The bar corresponds to a vertical scale of 24 nm for image (a) and of 6 nm for the other images.

From the x-ray diffraction analysis we thus conclude that the LBMO films grow single phased, epitaxially, and with a single out-of-plane orientation either on STO substrates or onto strained LSMO and SRO buffer layers.

### B. Morphology

In Fig. 4(a) we show the morphology of the surface of the LBMO single film. The material grows in a three-dimensional regime (Volmer–Weber mode) from the early stages of growth. The root-mean-square (rms) roughness of the layer is 2.2 nm. Figures 4(b) and 4(c) correspond to the morphologies of a LSMO single film and the LSMO/LBMO bilayer. The LSMO grows in a three-dimensional regime and shows a granular structure (with a rms roughness of 0.8 nm). The surface of the LSMO/LBMO bilayer reproduces the characteristics of the surface of the LSMO single film. Compared to what occurs when LBMO is grown in a single-film form, the roughness of the LBMO surface is strongly reduced when grown onto a LSMO buffer; the average lateral size of the islands decreases from 150 to 50 nm of size, and their average height drops from 8 to 3 nm.

Figures 4(d) and 4(e) show the morphology of the SRO single film and the LBMO/SRO bilayer, respectively. For the former, a clean terrace-like morphology is observed with steps having a height of 1.2 nm (3 unit cells). The surface of the bilayer is relatively smooth, too (with a rms roughness of 0.5 nm, to be compared to 0.4 nm for the SRO single layer).

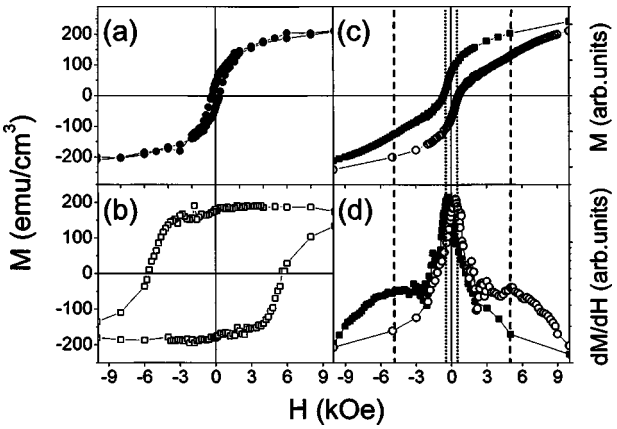


FIG. 5. Field dependence of the magnetization (at 10 K) of (a) a single LBMO films, (b) a single SRO film, and (c) a SRO/LBMO bilayer. The (d) panel shows the derivative of the M(H) curve of the SRO/LBMO bilayer.

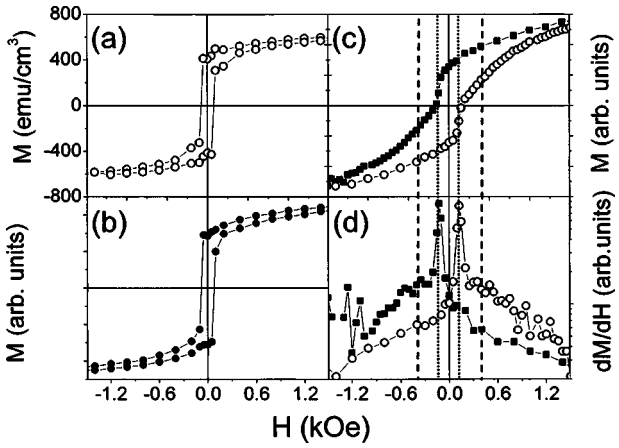


FIG. 6. Field dependence of the magnetization (at 10 K) of (a) a single LSMO films, (b) a LSMO/LBMO bilayer, and (c) a LSMO/STO/LBMO trilayer. The (d) panel shows the derivative of the M(H) curve of the LSMO/STO/LBMO trilayer.

The growth mode is three dimensional but the islands show an organization consistent with a nucleation along the step edges of the SRO buffer. The original structure of the steps is preserved as the lateral height modulation is on the order of two times the length of the steps of the SRO (380 nm for the bilayer versus 190 nm for the SRO single film).

The different morphologies observed for the LBMO when grown directly on STO or onto a LSMO or SRO buffer cannot result from a change in the elastic energy of the material as, in each case, the three surfaces we used for the growth show equivalent in-plane parameters, so the LBMO undergoes the same strain. Thus, this discrepancy of morphology is likely to result from the difference of wettability between the surfaces or from the size of the steps at the surfaces of the buffers. In this case, varying the miscut of the substrate would lead to a change in the growth mode of LBMO. This is the object of future work.

### C. Magnetic properties

As LBMO grows single phased and with a smooth surface on SRO and LSMO magnetic electrodes, it should be possible to use these structures as potential magnetic devices. To do so, it is important to be able to decouple magnetically the electrodes and the LBMO layer. In the following, we describe the magnetic properties (at 10 K) of the different heterostructures.

In Fig. 5(a), we plot the in-plane magnetization hysteresis loop of the LBMO single film. The loop displays a coercive field of 310 Oe with a saturation field of 20 kOe. The saturation magnetization is 250 emu cm$^{-3}$, which is approximately half the magnetization of bulk $BiMnO_3$ (Ref. 7), but in the range of what has been measured by Ohshima *et al.* for $BiMnO_3$ films of this thickness (30 nm).[8] In Fig. 5(b) we show the magnetic hysteresis loops of a SRO single film, the magnetization reversal of which occurs between 4 and 8 kOe. The saturation magnetization is about 200 emu cm$^{-3}$, close to the bulk moment (220 emu cm$^{-3}$). A hysteresis loop of a SRO/LBMO bilayer is presented in Fig. 5(c) and its derivative in Fig. 5(d). First, it is worth-mentioning that the saturation magnetization of the bilayer corresponds to the sum of the saturation magnetization of the single layers within an error of about 5%. One can notice two distinct magnetization jumps with their corresponding coercive fields. They are manifested as peaks in the dM/dH curve of Fig. 5(d) The first one is rather abrupt and takes place at 400 Oe and corresponds to the coercive field of the LBMO layer; the second one, much broader, occurs at 4 kOe and is due to the reversal of the SRO layer. By comparing these reversal field values with the coercive field measured on hysteresis loops of single layers, one can conclude that the reversal of the LBMO layer is uniform. The switching of the SRO layer is not as abrupt as for the SRO single film, which is indicative of some coupling with the LBMO layer. However, by setting the magnetic field to intermediate values in the 2-kOe range, it is possible to reach a highly noncollinear magnetization configuration of the two layers, which is essential to realize magnetic devices.

Similar measurements, with the field applied in plane, have been performed on LSMO-based samples. The hysteresis loop of a LSMO single film together with that of the LSMO/LBMO bilayer are respectively shown in Figs. 6(a) and 6(b). The former displays a coercive field of 70 Oe and a saturation magnetization of 600 emu/cm$^3$ (similar to that of bulk LSMO). In Fig. 6(b) we show the magnetization loop of the LSMO/LBMO bilayer. No evidence of independent switching of both layers is found, as only the switching of the LSMO buffer is visible around 70 Oe. The two magnetic layers appear to be ferromagnetically coupled. In order to decouple magnetic layers, the most straightforward method is to insert a nonmagnetic spacer. Consequently, we have grown analogous heterostructures inserting a 1.2-nm layer of STO between the LSMO and LBMO layers. The thickness of the LSMO layer for this sample was 25 nm. The magnetization loop of the LSMO/STO/LBMO trilayer is presented in Fig. 6(c) together with its derivative in function of the applied field. Even though the effect is not as clear as for the SRO/LBMO bilayer, one can notice two distinct magnetization reversals on the hysteresis confirmed by peaklike features present in the derivative [Fig. 6(d)]. The sharp variation detected at 120 Oe can be attributed to the reversal of the LSMO layer, as it is close to the value of the coercive field

obtained for 25-nm single films. The other feature is much broader and shows a maximum at about 400 Oe. It corresponds to the rotation of the magnetization of the LBMO layer. This value is the same as that obtained for the LBMO single film. For this heterostructure, the values of the reversal fields are closer to each other than for the SRO/LBMO bilayer. However, we can conclude that it is still possible to obtain decoupled LSMO and LBMO layers by inserting a thin STO spacer between them.

## IV. SUMMARY AND CONCLUSION

In summary, we have grown films of the $La_{0.1}Bi_{0.9}MnO_3$ ferromagnetic-insulating perovskite. Despite the presumed monoclinic symmetry of the bulk compound, the films are found to grow epitaxially and with a single orientation onto $SrTiO_3$ (001) single crystals or ferromagnetic-metallic $La_{2/3}Sr_{1/3}MnO_3$ and $SrRuO_3$ epitaxial buffers. The morphology of the single films is rather rough but becomes much smoother when grown onto the buffers. The LBMO films are ferromagnetic at low temperature and their magnetization, although lower than that expected for the bulk compound, can be decoupled from that of the underlying ferromagnetic buffers. Although experimental demonstration of ferroelectricity in this coumpound is still lacking, these results show that our LBMO-based heterostructures fulfill the requisites desired for their use as magnetoelectric and/or spin-polarized tunneling devices.

## ACKNOWLEDGMENTS

This work has been supported in part by the MCyT (Spain) project (Project No. MAT2002-03431), FEDER, and the Franco-Spanish project (Project No. HF-20020090). M.G. acknowledges financial support from ICMAB through the Marie Curie Training Site program. The authors would like to thank R. Bisaro for his help for x-ray diffraction measurements.

[1] N. A. Hill, J. Phys. Chem. B **104**, 6694 (2000).
[2] G. A. Smolenski and I. E. Chupis, Sov. Phys. Usp. **25**, 475 (1983).
[3] T. Goto, T. Kimura, G. Lawes, A. P. Ramirez, and Y. Tokura, Phys. Rev. Lett. **92**, 257201 (2004).
[4] N. Hur, S. Park, P. A. Sharma, J. S. Ahn, S. Guha, and S.-W. Cheong, Nature (London) **429**, 392 (2004).
[5] J. Wang *et al.*, Science **299**, 1719 (2003).
[6] I. O. Troyanchuk, O. S. Mantytskaja, H. Szymczak, and M. Y. Shvedun, Low Temp. Phys. **28**, 569 (2002).
[7] T. Kimura, S. Kawamoto, I. Yamada, M. Azuma, M. Takano, and Y. Tokura, Phys. Rev. B **67**, 180401 (2003).
[8] E. Ohshima, Y. Saya, M. Nantoh and M. Kawai, Solid State Commun. **116**, 73 (2000).
[9] A. Moreira dos Santos, A. K. Cheetam, W. Tian, X. Pan, Y. Jia, N. J. Murphy, J. Lettieri, and D. G. Schlom, Appl. Phys. Lett. **84**, 91 (2004).
[10] M. Gajek *et al.* (unpublished).
[11] H. Chiba, T. Atou, and Y. Syono, J. Solid State Chem. **132**, 139 (1997).